Broadband Seismology and Small Regional Seismic Networks

U.S. GEOLOGICAL SURVEY PROFESSIONAL PAPER 1538–S

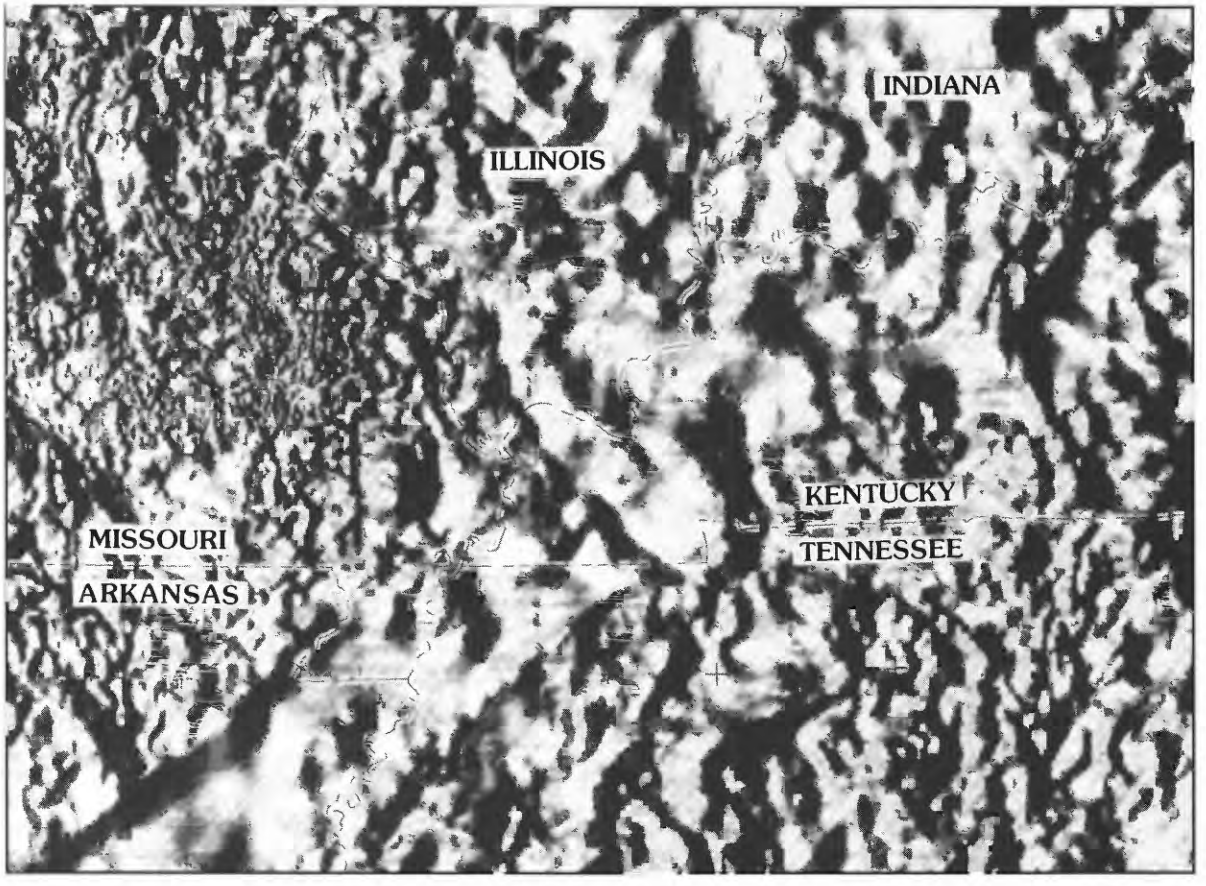

Cover. Gray, shaded-relief map of magnetic anomaly data. Map area includes parts of Missouri, Illinois, Indiana, Kentucky, Tennessee, and Arkansas. Illumination is from the west. Figure is from *Geophysical setting of the Reelfoot rift and relations between rift structures and the New Madrid seismic zone*, by Thomas G. Hildenbrand and John D. Hendricks (chapter E in this series).

Broadband Seismology and Small Regional Seismic Networks

By R.B. Herrmann

INVESTIGATIONS OF THE NEW MADRID SEISMIC ZONE
Edited by Kaye M. Shedlock *and* Arch C. Johnston

U.S. GEOLOGICAL SURVEY PROFESSIONAL PAPER 1538–S

UNITED STATES GOVERNMENT PRINTING OFFICE, WASHINGTON : 1995

U.S. DEPARTMENT OF THE INTERIOR
BRUCE BABBITT, Secretary

U.S. GEOLOGICAL SURVEY
Gordon P. Eaton, Director

For sale by U.S. Geological Survey, Information Services
Box 25286, Federal Center
Denver, CO 80225

Library of Congress Cataloging-in-Publication Data

Herrmann, Robert B.
Broadband seismology and small regional seismic networks / by R.B. Herrmann.
p. cm.—(Investigations of the New Madrid seismic zone ; S)
(U.S. Geological Survey professional paper, 1538–S)
Includes bibliographical references.
Supt. of Docs. no. : I19.16:1538S
1. Earthquakes—Missouri—New Madrid Region. 2. Seismology—Missouri—New Madrid Region. I. Title. II. Series. III. Series: U.S. Geological Survey professional paper ; 1538.
QE535.2.U6I59 1995 vol. S
551.2'2'09778985 s—dc20
[551.2'2'0978985] 95–5245
CIP

CONTENTS

FIGURES

TABLES

BROADBAND SEISMOLOGY AND SMALL REGIONAL SEISMIC NETWORKS

By R.B. Herrmann[1]

ABSTRACT

The New Madrid seismic zone earthquakes of September 26, 1990, and May 4, 1991, are analyzed from the point of view of demonstrating how broadband digital recordings at regional distances can be used together with regional-seismic-network data to define source parameters and Earth structure. Regional-seismic-network data provide excellent epicenter information, and broadband data provide seismic moment values. In addition, the broadband data can provide strong constraints on both the focal mechanism, when focal-sphere coverage of regional network data is sparse, and the source depth, when the epicenter is not well situated with respect to network geometry.

The September 26, 1990, earthquake has a source depth of 15 km and a seismic moment of 3.5×10^{22} dyne-cm. The focal mechanism is primarily one of thrust faulting, with the pressure axes aligned roughly east-west. One nodal plane strikes 145° and dips 75° SW., and the other strikes 20° and dips 25° SE. The broadband-waveform-fit depth agrees well with aftershock monitoring.

The May 4, 1991, earthquake near Risco, Mo., had a source depth of 8 km, which was well constrained by the PANDA (portable array for numerical data acquisition) (Chiu and others, 1991) deployment. The seismic moment is estimated to be 1.7×10^{22} dyne-cm. The focal mechanism indicates predominantly strike-slip faulting, with the P-axis trending northeast-southwest. One nodal plane strikes 353° and dips 66° E., and the other strikes 90° and dips 75° S.

Both focal mechanisms obtained are compatible with previous solutions in the seismic zone. In addition, there is evidence of 3 percent variation in crustal velocities over slightly different paths.

[1]Department of Earth and Atmospheric Sciences, Saint Louis University, 3507 Laclede Avenue, St. Louis, MO 63103.

INTRODUCTION

The New Madrid seismic zone includes the locations of three very large earthquakes (m_b>7.0) that occurred during the winter of 1811–12. Most of the larger earthquakes (m_b>5.2) in the Central United States since then have occurred in this zone (Mitchell and others, 1991). Focal mechanisms have been obtained for a number of the modern earthquakes. When combined with other crustal-stress data, earthquake focal mechanisms in the region are consistent with E.-W. or ENE.-WSW. orientations of maximum compressive stress (Zoback and Zoback, 1991; Zoback, 1992). Some previously inconsistent focal mechanisms were revised by Herrmann (in press) and are now consistent with this overall trend. Given this agreement, the object of focal-mechanism studies now is on the relation of nodal planes to spatial seismicity patterns and on the dependence of strong ground motion on the particular mechanism.

Regional seismic activity has been monitored by a variety of seismographs since the installation of the 80-kg Wiechert seismograph at Saint Louis University in 1909. Significant milestones in instrumentation were the installations of the WWSSN (World Wide Standard Seismograph Network) long-period instrument in the 1960's, the regional seismic network in 1975, the broadband digital IRIS (Incorporated Research Institutions for Seismology) station at CCM (Cathedral Cave, Mo.) in 1989, and the local deployment of the dense PANDA array in 1989–92 (Yang and others, in press).

The object of this paper is to derive source parameters for two large earthquakes that occurred in the zone during 1990–91 and to assess how regional network data can complement broadband digital data. The two earthquakes are those of September 26, 1990, and May 4, 1991. The origin times and locations of these events are given in table 1. Figure 1 shows the location of these two events with respect to the regional network seismicity. In addition, the location of the IRIS station CCM is indicated. The May 4, 1991, earthquake is close to the dense linear patterns of seismicity near New Madrid, Mo., whereas the September 26, 1990, earthquake is on the periphery of the very active zone (fig. 1). The

Table 1. Event information for earthquakes in the New Madrid seismic zone on September 26, 1990, and May 4, 1991.

[UT, Coordinated Universal Time. CUS crustal model derived from Nuttli and others (1969). MALDEN crustal model is the result of modeling Rayleigh- and Love-wave signals as a single-mode surface wave]

Date	Origin time (UT)	Latitude	Longitude	Depth (km)	Strike (degrees)	Dip (degrees)	Rake (degrees)	Moment (dyne-cm)	Model
09/26/90	13:18	37°09.6'N.	89°34.8'W.	15	145	75	70	3.5×10^{22}	CUS
05/04/91	01:18	36°33.6'N.	89°49.8'W.	8	90	75	20	2.0×10^{22}	CUS
				8	90	75	25	1.7×10^{22}	MALDEN

Table 2. Parameters of layered elastic halfspace for CUS and MALDEN models used in generation of synthetic seismograms.

[H, layer thickness; V_P, P-wave velocity; V_S, S-wave velocity; ρ, density; Q_P^{-1}, inverse P-wave quality factor; Q_S^{-1}, inverse S-wave quality factor]

H (km)	V_P (km/s)	V_S (km/s)	ρ (g/cm^3)	Q_P^{-1}	Q_S^{-1}
CUS crustal model					
1.00	5.0	2.89	2.5	0.005	0.01
9.00	6.1	3.52	2.7	0.0005	0.001
10.00	6.4	3.70	2.9	0.0005	0.001
20.00	6.7	3.87	3.0	0.0005	0.001
	8.15	4.70	3.4	0.0005	0.001
MALDEN crustal model					
1.00	4.89	2.83	2.5	0.005	0.01
9.00	5.98	3.44	2.7	0.0005	0.001
10.00	6.21	3.59	2.8	0.0005	0.001
10.00	6.44	3.72	2.8	0.0005	0.001
10.00	6.47	3.74	2.8	0.0005	0.001
20.00	7.97	4.60	3.3	0.0005	0.001
	8.05	4.65	3.3	0.0005	0.001

seismograph-station distribution of the regional network roughly parallels the density of the seismicity.

EARTHQUAKE OF SEPTEMBER 26, 1990

This earthquake is interesting for a number of reasons. First, its location is along a diffuse northwest seismicity trend to the north of the strong linear seismicity trends of the central portion of the New Madrid seismic zone (fig. 1). In addition, the m_{Lg}=4.5 earthquake occurred at the edge of the regional seismic network, 31 km away from the nearest seismograph station. Thus, depth control is poor because it depends on sensitivity to first-arrival-cross-over distances of the particular crustal model used rather than to the curvature of the travel-time curve and good S-P arrival-time differences at short distances. Finally, because of the lack of seismograph stations directly above the source, the focal-sphere coverage of P-wave first-motion data is not sufficient to completely define the nodal planes of the focal mechanism.

The broadband signal at CCM, a distance of 175 km at an azimuth of 305°, was passed through a WWSSN

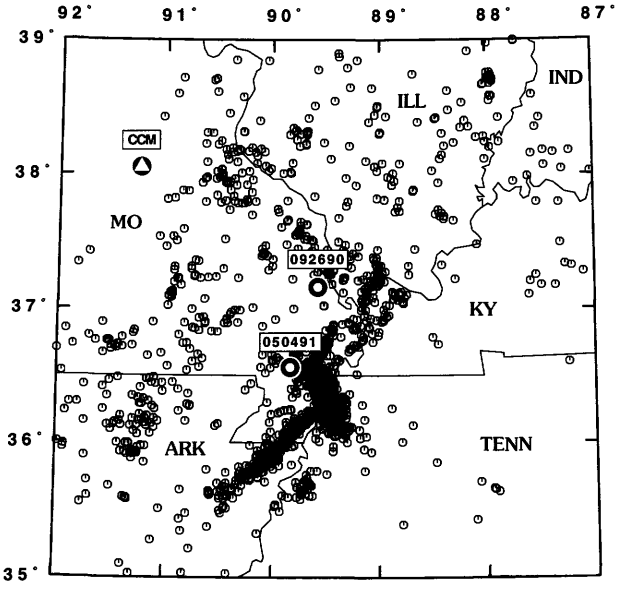

Figure 1. Location of the September 26, 1990, (092690), and May 4, 1991, (050491), earthquakes in the New Madrid seismic zone in relation to the seismicity contained in the regional-seismic-network catalog from 1975–92. The location of IRIS station CCM is indicated.

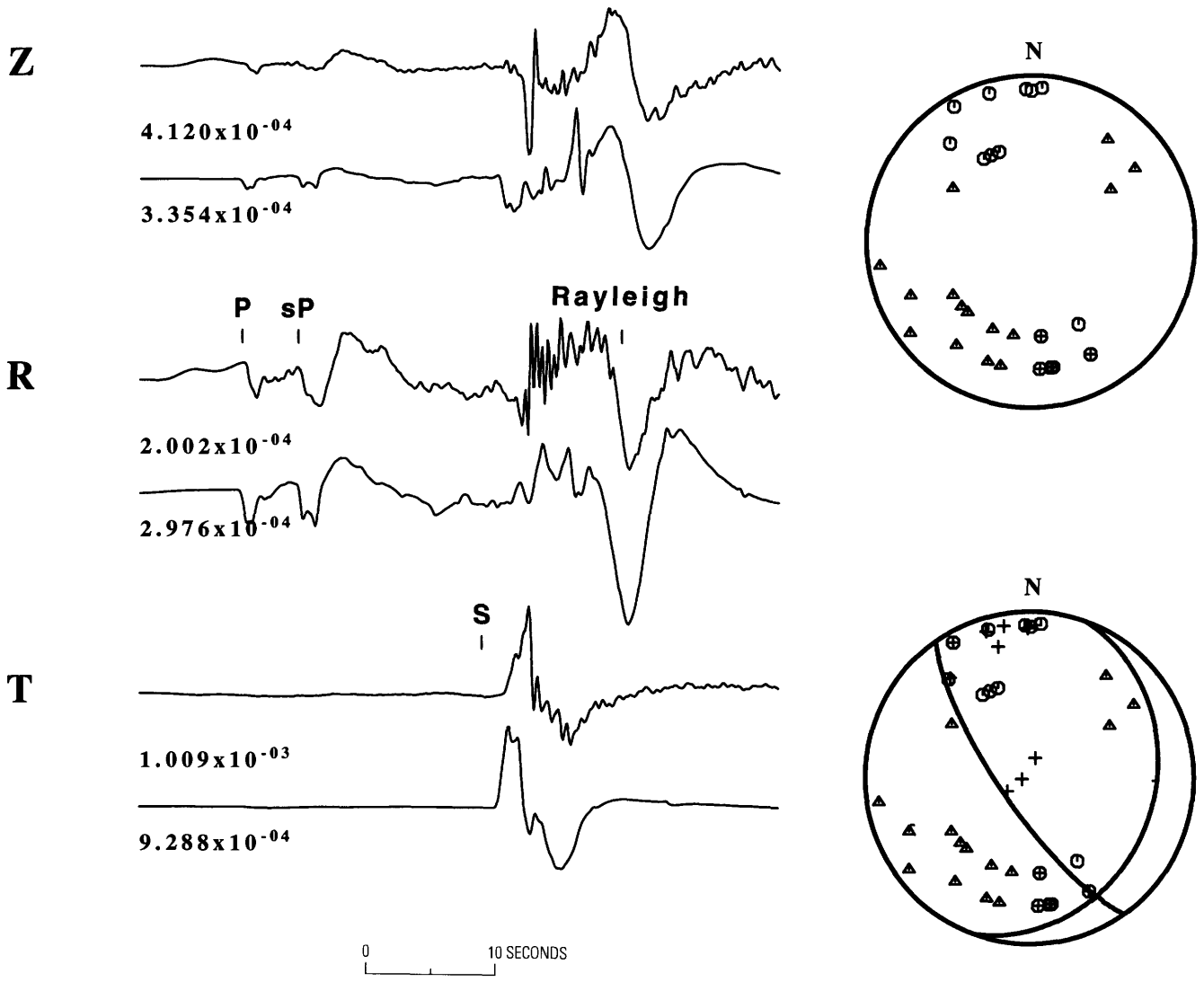

Figure 2. Comparison of observed and synthetic (upper and lower traces, respectively, for each component) time histories for the September 26, 1990, earthquake recorded at IRIS station CCM. Both sets are filtered using a 15-100 WWSSN LP instrument response with a peak gain of 1. Peak amplitudes have units of centimeters. A total of 50 s of displacement time history is displayed, starting 20 s after the event origin time. Each pair of observed and synthetic traces is plotted using the same linear scale to emphasize similarity of modeled phases. The source parameters used in making the synthetics are given in table 1 for this earthquake. The lower-hemisphere equal-area projections to the right show the observed P-wave first-motion data from the main event (upper) and the main and aftershock first-motion data (lower). The mechanism plotted is that required by the waveform fit. A circle or plus sign indicates a compression, and a triangle or minus sign indicates a dilatation. Positive Z, R, and T component values represent motion up, away from the source, and in a direction clockwise around the source.

15-100 instrument response with a peak gain of 1.0 to make equivalent seismograms. These observed three-component seismograms are shown as the upper traces in each part of figure 2. Shown in the upper-right-hand corner of figure 2 are the observed P-wave first-motion data for the earthquake plotted in a lower-hemisphere equal-area projection. As can be seen, a number of focal mechanisms can be placed through these observations, depending on the number of inconsistencies permitted.

To use the broadband signal to constrain the focal mechanism, synthetic seismograms were generated using the CUS model of table 2. This model is derived from the simple crustal model given by Nuttli and others (1969) and used for synthetic seismogram modeling (Herrmann, 1979a) and focal mechanism determination from surface waves (Herrmann, 1979b). The model does a reasonable job in explaining surface-wave group velocity dispersion in the 5- to 50-s period range in the Midcontinent. Wavenumber integration code was used to generate synthetic seismograms. Rather than attempt a true waveform inversion for source parameters and structure, synthetic seismograms were generated for a suite of strike, dip, and rake values for

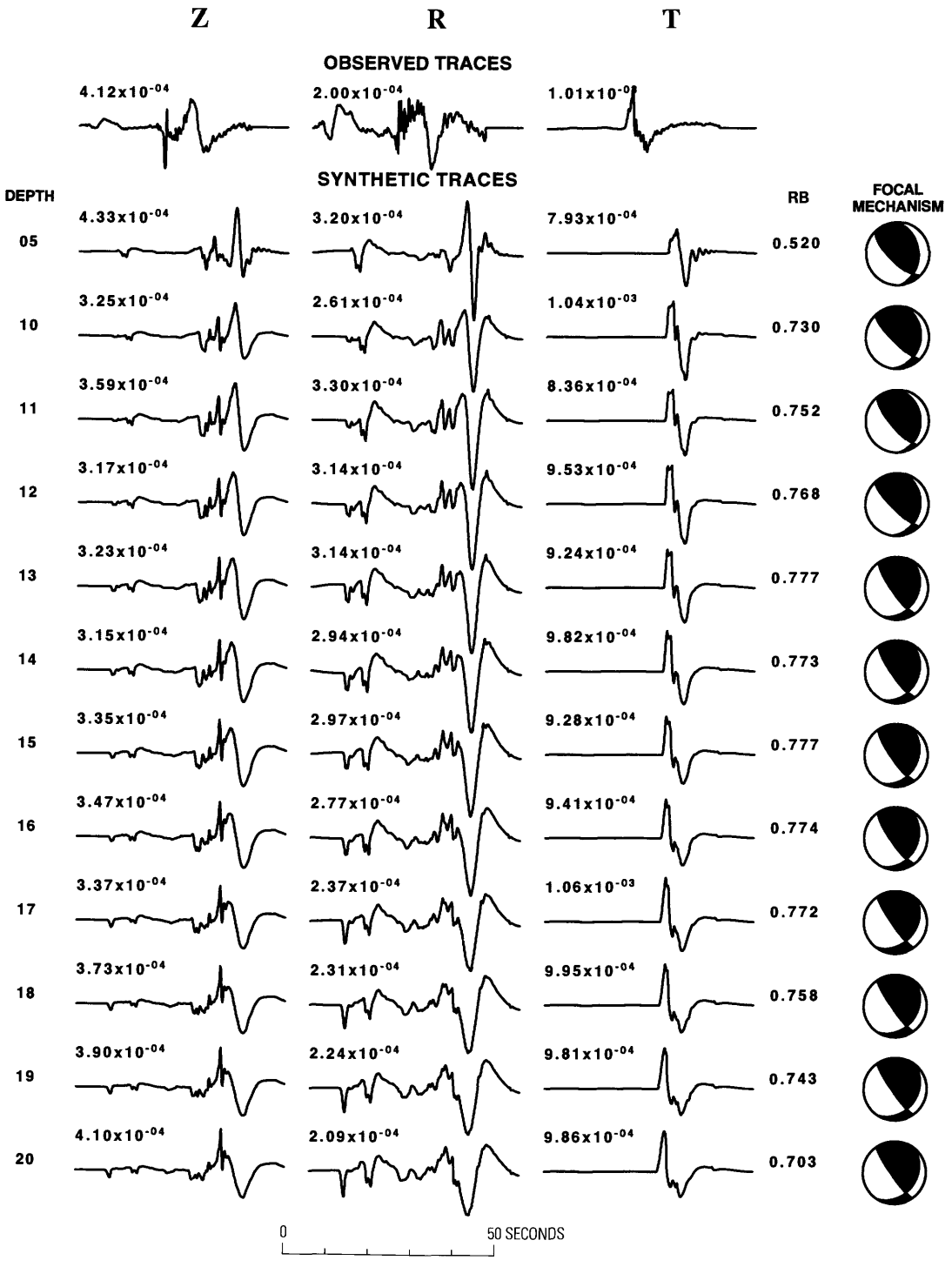

Figure 3. Comparison of observed and synthetic seismogram time histories for different source depths (shown in kilometers) in CUS Earth model for the September 26, 1990, earthquake. All time histories are filtered with the WWSSN LP instrument response as in figure 2. Observed traces are plotted in the top row. Other rows are the best solutions using the grid search method for focal depths of 5 to 20 km. The grid search goodness-of-fit value, RB, is given to the right of the synthetic traces. The corresponding lower-hemisphere-projection focal mechanism, in which the compressional quadrant is shaded, for each depth is plotted to the right of RB values. All traces present 50 s of time history, starting 20 s after the origin time. Positive Z, R, and T component values represent motion up, away from the source, and in a direction clockwise around the source.

a double-couple source at different depths. The choice of the strike, dip, and rake angles was initially based on visual examination of P-wave first-motion data in figure 2.

A visual goodness-of-fit criteria is based on several observations of the observed signals. First, the P-wave first-motion is a dilatation. Second, the phase approximately 5 s after P (identified as "sP" by Langston, 1994) is also a dilatation. Third, the first motion on the tangential component is positive. Fourth, the ratio of peak amplitudes on the Z, R, and T components is roughly 1, 1, and 5, respectively (ignoring the high-frequency spike on the Z component, which depends on the fine detail of the velocity structure in the lower crust and upper mantle). Finally, the shape of the Rayleigh-wave pulse on the Z and R components must agree. Even though this qualitative set of criteria is difficult to quantify, the final solution is very sensitive to changes in strike, dip, and rake angles of 10°.

After finding a good visual fit, the grid search technique (described in the Appendix) is used to strictly obtain the best fit. In doing this, a computationally intensive grid search uses a restricted range of focal-mechanism parameters that were chosen on the basis of the initial visual search. The search grid included dip angles every 5° in the inclusive range of 60°–90°, strike angles every 5° in the range 135°–180°, rake angles every 5° in the range 55°–110°, and source depths from 5–20 km in increments of 1 km.

Figure 3 shows the best fit at each source depth between observed and predicted time histories. The goodness-of-fit parameter, RB (see Appendix), is indicated to the left of the lower-hemisphere focal-mechanism diagram. The RB reaches a maximum at depths of 13 and 15 km. This sequence of computations highlights those features of the waveforms that are sensitive to depth. First, the separation between P and sP increases with depth on the Z and R components. Second, the high-frequency spike in the vertical-component synthetics (component Z) is depth sensitive in arrival time and must be due to an initial upward-propagating S wave from the source. Next, the width of the Rayleigh-wave pulse increases with depth. The 5-km depth trace in figure 3 is visually rejected from being the best fit to the observed time histories because of these observations. It is also rejected by the low RB value. The Earth model used is not capable of accounting for the high-frequency spike on the vertical component, but grid searches using other Earth-structure models do not yield very different focal mechanism and depth selections.

The accepted focal-mechanism solution for the September 26, 1990, earthquake is listed in table 1 and plotted in the lower right of figure 2. This solution has only seven P-wave first motion inconsistencies for the main shock. It is also consistent with aftershock data, indicated by the focal mechanism displayed at the lower right part of figure 2 (of course, this assumes that the aftershocks and the main event have the same focal mechanisms). The first-motion inconsistencies may be due to an imperfect Earth model, which is evidenced by the mismatch of the S-wave pulses on the vertical (Z) component. The other feature of the solution is that the focal depth is in the 13- to 15-km range rather than at 10 or 20 km. This is consistent with focal depths of 10–16 km for aftershocks located using regional network data as well as readings from portable instruments deployed above the hypocenter (Taylor and Wuenscher, 1990).

The Langston (1994) focal mechanism for this event had about the same seismic moment and had one nodal plane striking 50° and dipping 60° SE. and the other nodal plane striking 153° and dipping 68° SW. The solution given in table 1 has one nodal plane striking 20° and dipping 25° SE. and the other striking 145° and dipping 75° SW. Both solutions have approximately east-west pressure axes. The Langston (1994) Earth model provides a better fit to the high-frequency S pulse on the Z component, but his model predicts an sP/P ratio on the R component that is greater than that observed. Although the focal mechanisms are very similar, the differences are due to the Earth model used and also to the complexity of the search technique used, the search technique of this paper being computationally more intensive.

EARTHQUAKE OF MAY 4, 1991

This earthquake occurred near the towns of Risco and Malden, Mo., and occurred well within the station distribution of the New Madrid regional seismic network and also within the dense PANDA deployment (Yang and others, in press). Because of this location relative to the two seismic networks, the focal depth of the event is well defined and is given as 6.9 km by Yang and others (in press). In addition, the focal mechanism is relatively well constrained.

Figure 4 presents the observed P-wave first-motion data, the observed seismograms, and the synthetic seismograms for CCM that fit the data well. The dip of the east-west nodal plane of figure 4 is not well constrained from the first-motion data, and can vary in dip from south to north, but is constrained by the waveform data. For this event, the distance to CCM is 209 km along an azimuth of 323°.

The grid search technique was again applied, with dip angles varying from 60° to 75° in increments of 5°, the strike varying from 70° to 110° in increments of 5°, and the rake angle varying from –20° to 40° in increments of 5°. Depths were sampled in the range of 5 to 20 km. Figure 5 shows the results of the grid search, plotting the synthetic time history for the best fitting focal mechanism at each depth. The RB values indicate that the best fit to the observed waveforms is obtained at a source depth of 8 km. Because the sP phase is not as prominent as in the previous example (fig. 3) because of focal mechanism, the major constraint on source depth is the pulse width of the Rayleigh-wave pulse on the Z and R components. Figure 5 shows the sensitivity of the synthetic time histories to focal depth, which is permitted to vary from 5 to 20 km. The 8-km depth chosen for this earthquake is

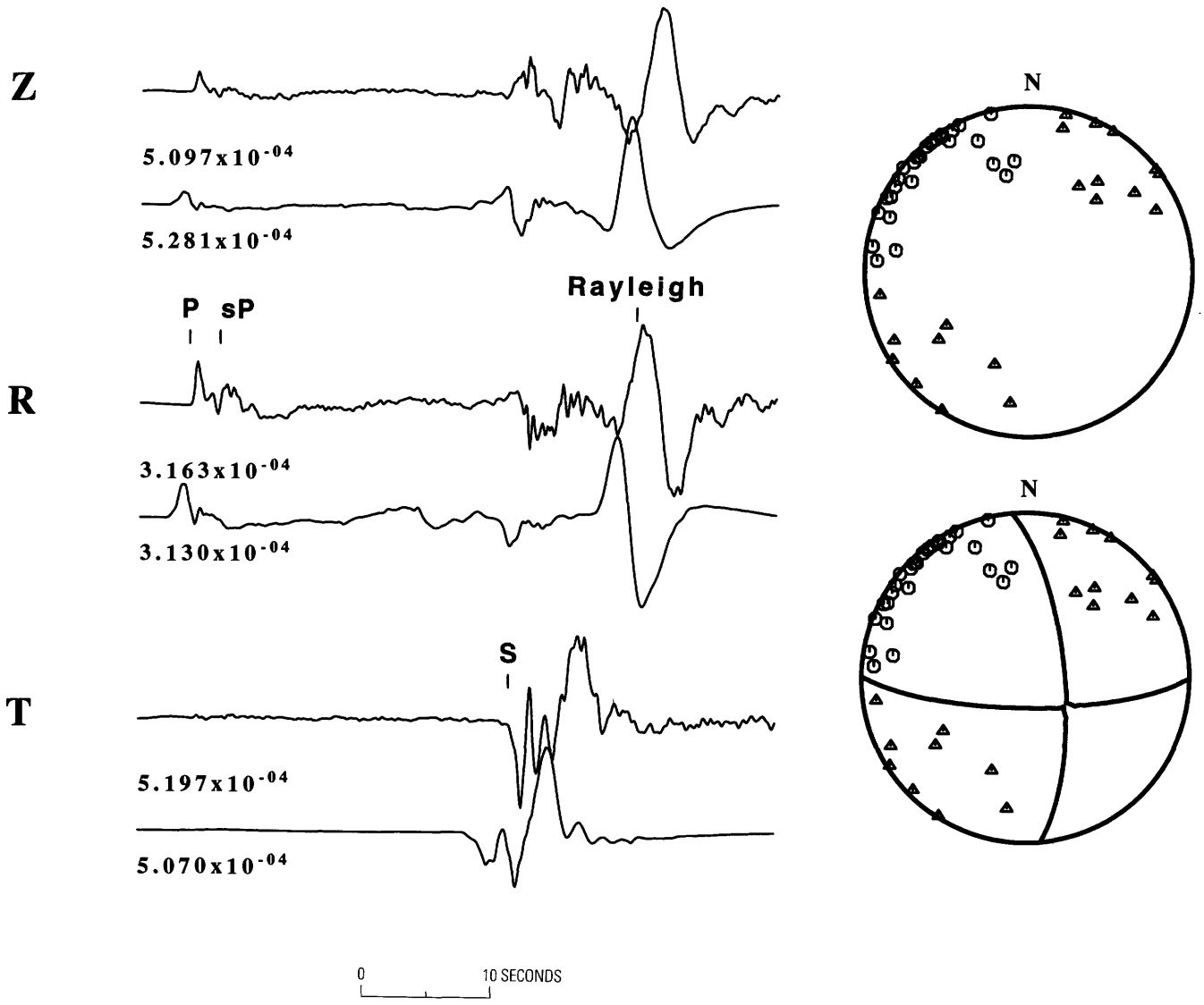

Figure 4. Comparison of observed and synthetic (upper and lower traces, respectively, for each component) time histories for the May 4, 1991, earthquake recorded at IRIS station CCM. Both sets are filtered using a 15-100 WWSSN LP instrument response with a peak gain of 1. Peak amplitudes have units of centimeters. A total of 50 s of time history is displayed, starting 30 s after the event origin time. Each pair of traces is plotted using the same scale for comparison of individual features. The source parameters used in making the synthetics are given in table 1 for this earthquake and the CUS structure. The lower-hemisphere equal-area projections to the right show the observed P-wave first-motion data from the event with (upper) and without (lower) the focal mechanism superimposed. Circles and triangles indicate compressional or dilatational P-wave first-motion, respectively. The CUS model is used. Positive Z, R, and T component values represent motion up, away from the source, and in a direction clockwise around the source.

seen to provide a reasonable agreement in the duration of the Rayleigh wave.

The selected best solution is given in table 1, and the corresponding synthetic traces are plotted in figure 4. Several observations can be made by comparing the traces. The Rayleigh and S arrivals are predicted too early by the model, even though the shape and amplitudes of the prominent arrivals are in agreement. Additionally, the shape of the Rayleigh pulse on the Z component is slightly out of phase with the synthetic time history.

To reconcile the problems with the Rayleigh- and S-wave arrival times, the arrivals were modeled as a single-mode surface wave, and the phase difference in the complex signal was used to define an improved phase-velocity dispersion between the source and receiver, and thus lead to a better Earth model (see Appendix). The result is the MALDEN model of table 2. The difference between this model and the CUS model is that the shear-wave velocity is lower throughout the entire crust by about 0.1 km/s, or about 3 percent (Langston, 1994, also noted the need for a slower model but, instead of defining a new model, simply

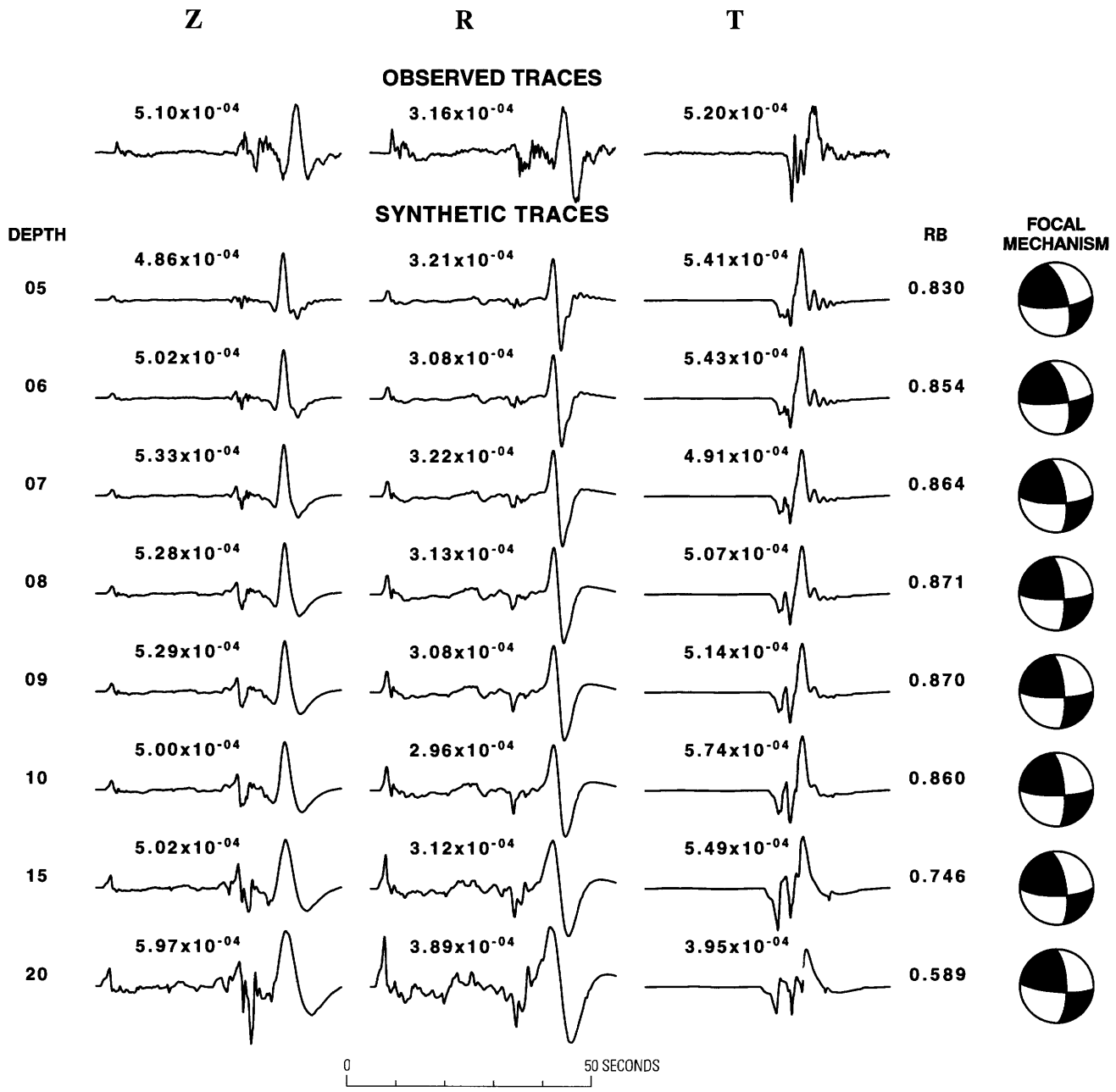

Figure 5. Comparison of observed and synthetic seismogram time histories for different source depths in CUS Earth model for the May 4, 1991, earthquake. The observed traces are given in the top row, with the other rows giving the solution for different source depths (shown in kilometers). The grid search goodness-of-fit parameter (RB) and focal mechanism are also indicated. All traces start 30 s after the origin time and consist of 50-s segments. Positive Z, R, and T component values represent motion up, away from the source, and in a direction clockwise around the source.

constructed synthetics at a distance of 220 km to improve phase alignment). The best fitting synthetic time histories for the MALDEN model are shown in figure 6. Note the better agreement in the arrival time of the large positive amplitudes on the three components as well as the phase of the Rayleigh-wave pulse on the Z component. Figure 7 shows the results of the grid search for a limited selection of source depths. The best focal mechanism and corresponding seismic moment differ slightly from that obtained using the CUS model (table 2).

DISCUSSION

The focal mechanisms obtained here are similar to those found in Langston (1994) but differ somewhat because

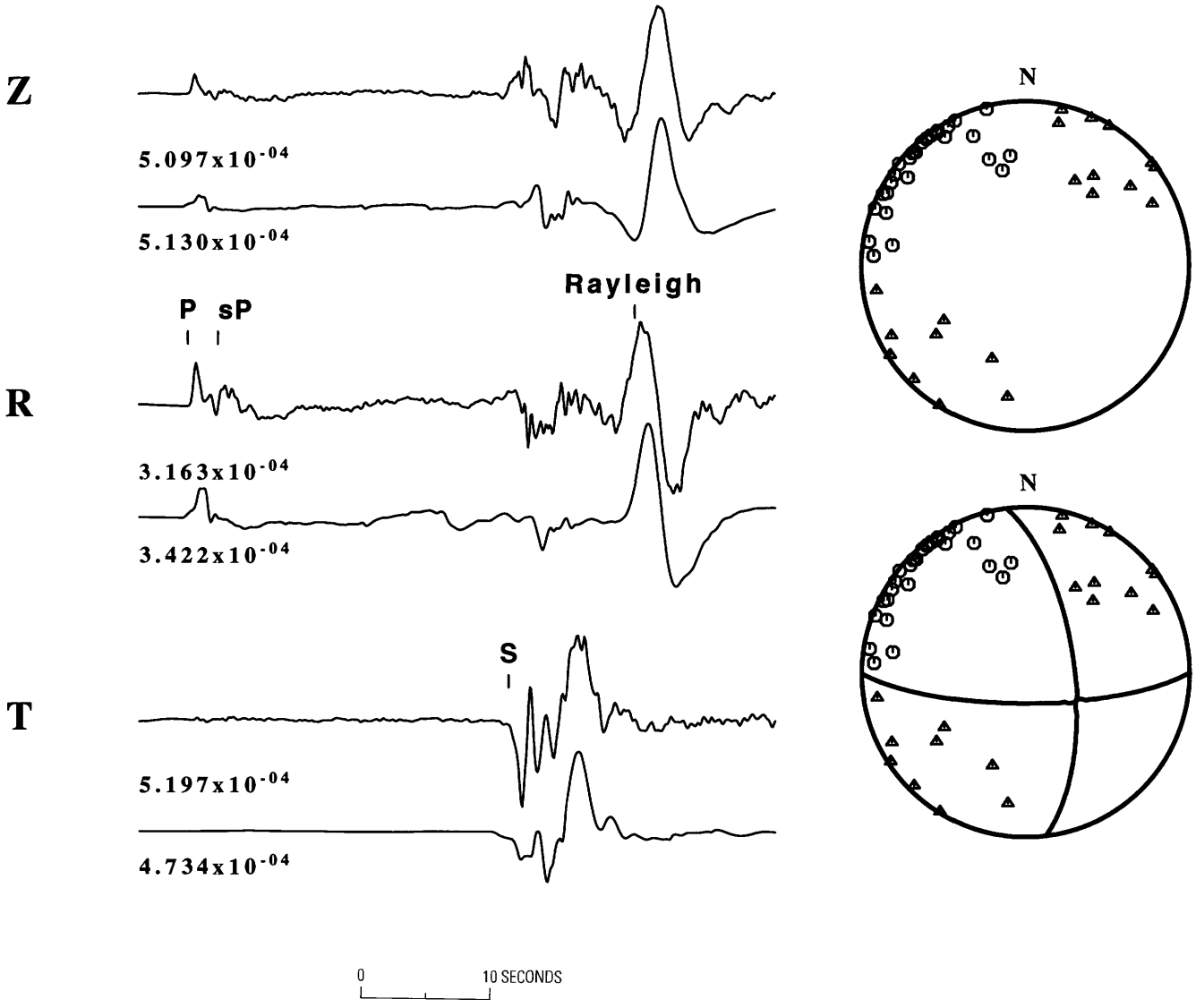

Figure 6. Comparison of observed and synthetic (upper and lower traces, respectively, for each component) time histories for the May 4, 1991, earthquake recorded at IRIS station CCM. Both sets are filtered using a 15-100 WWSSN LP instrument response with a peak gain of 1. Peak amplitudes have units of centimeters. The source parameters used in making the synthetics are given in table 1 for this earthquake and the MALDEN structure derived from these observed waveforms. The first-motion information is described in figure 4. The MALDEN model is used. Note the better agreement in arrival time and phase of the surface waves compared with that shown in figure 4. Positive Z, R, and T component values represent motion up, away from the source, and in a direction clockwise around the source.

of the nature of his shear-wave velocities in the lower crust. This study was not a direct attempt at waveform linear inversion, but rather it is an initial study to understand the salient features of the waveform to be fit. A numerical goodness-of-fit procedure was implemented in order to quantify a good fit. Regional-seismic-network data were necessary to provide a first-order constraint on focal mechanisms through P-wave first-motion data and through depth estimates. Even though the waveforms themselves are capable of defining depth, an initial estimate of values is required to generate the Green's functions used for constructing synthetic seismograms.

To see how these focal mechanisms agree with other solutions in the region, they are plotted together with seismicity in figure 8. The other focal mechanisms, including corrected mechanisms for the July 21, 1967, earthquake at the upper left corner of the figure, and the March 3, 1963, earthquake just west of the May 4, 1991, earthquake are taken from Herrmann (1979b, in press). The May 4, 1991, earthquake lies on an east-west seismicity trend, and, on the basis of this, the east-west-striking nodal plane can be assumed to be the fault plane. The September 26, 1990, earthquake is plotted at the top center of the figure. It is associated with a diffuse pattern of seismicity. However,

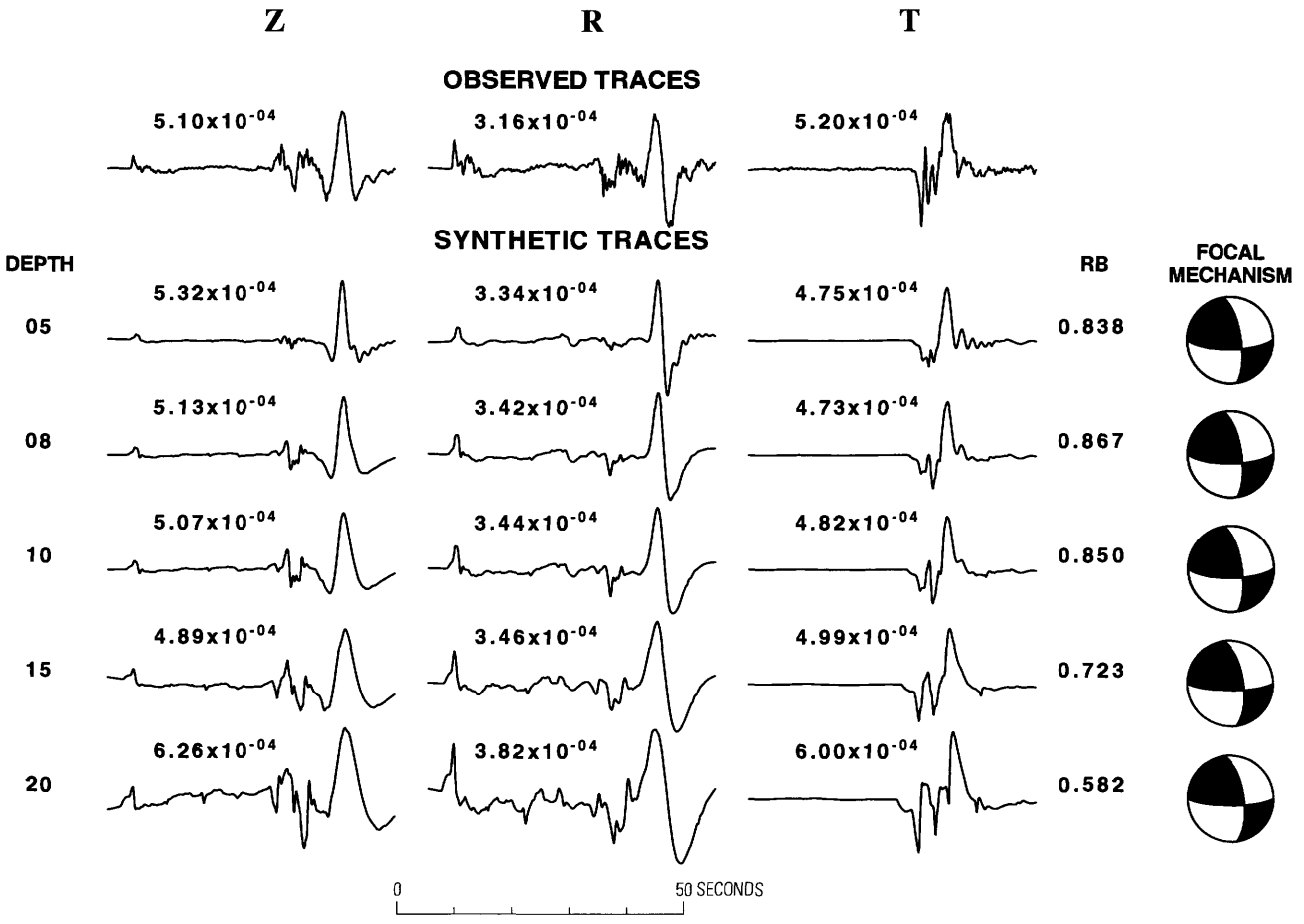

Figure 7. Comparison of observed traces to synthetics for different source depths in the MALDEN Earth model for the May 4, 1991, earthquake. The presentation is identical to that of figure 5.

the east-west-trending P-axis is consistent with the other mechanisms in the area and also with compressive stress patterns in the Midcontinent (Zoback and Zoback, 1991; Zoback, 1992).

An interesting feature of the study is the sensitivity of the long-period portion of broadband data to Earth structure. The CUS model was adequate for describing most features of the observed waveform of the September 26, 1990, earthquake. However, it was not able to describe the high-frequency arrival following S on the R component and the large-amplitude S pulse on the Z component. To illustrate this, figure 9 compares the observed and synthesized ground velocities after being low-pass-filtered with different corner frequencies. The source parameters of table 1 were used together with the CUS Earth model. As higher frequencies are introduced by increasing the filter corner frequency, the agreement between the observed and synthetic waveforms decreases in terms of shape, frequency content, and peak amplitude. This is not unexpected because the Earth model used is a very simple, plane-layered structure. Preliminary attempts at waveform inversion for velocity structure indicates that changes are required in both the entire crust and in the upper mantle to better explain the high-frequency character of the waveforms.

The problem of an appropriate velocity model is interesting. This paper has shown evidence that the Earth models required to fit waveforms recorded at the same seismograph station from two earthquakes, separated by only 70 km, must vary by 2–4 percent in velocity (comparison of CUS and MALDEN models in table 2). This difference in structure along two neighboring paths is not unexpected, given that the May 4, 1991, earthquake occurred near the edge of the Reelfoot graben and intrusive plutons (Hildenbrand and others, 1992). In the future, data from additional stations will make it possible to determine whether this velocity change is uniform over the entire path or if it is spatially variable. Information on the lateral variation of the crustal-velocity model may provide crucial information to explain the occurrence of earthquakes in the region. Finally, the difference in high-frequency-waveform detail indicates the need to refine the models in order to improve predictions of high-frequency ground motion for hazard mitigation.

ACKNOWLEDGMENTS

This research was sponsored in part by the U.S. Geological Survey under grants 14-08-0001-G2138 and 14-08-0001-G2142 and by Phillips Laboratory, Hanscom AFB under contract F19628-90-K-0040. This paper benefited from the suggestions of H. Kanamori, K. Shedlock, and an anonymous reviewer.

REFERENCES CITED

Chiu, J.M., Steiner, G., Smalley, R., Jr., and Johnston, A.C., 1991, PANDA: A simple, portable seismic array for local- to regional-scale seismic experiments: Bulletin of the Seismological Society of America, v. 81, no. 3, p. 1000–1014.

Herrmann, R.B., 1979a, SH-wave generation by dislocation sources—A numerical study: Bulletin of the Seismological Society of America, v. 69, no. 1, p. 1–15.

———1979b, Surface wave focal mechanisms for eastern North American earthquakes with tectonic implications: Journal of Geophysical Research, v. 84, no. B7, p. 3543–3552.

———in press, Broadband modeling of regional seismic events: Bulletin of the Seismological Society of America, v. 85.

Hildenbrand, T.G., Rosenbaum, J.G., and Reynolds, R.L., 1992, High-resolution aeromagnetic study of the New Madrid seismic zone: A preliminary report: Seismological Research Letters, v. 63, no. 3, p. 209–232.

Jenkins, G.M., and Watts, D.G., 1968, Spectral Analysis and its Applications: San Francisco, Holden-Day, 525 p.

Langston, C.A., 1994, An integrated study of crustal structure and regional wave propagation for southeastern Missouri: Bulletin of the Seismological Society of America, v. 84, no. 1, p. 105–118.

Mitchell, B.J., Nuttli, O.W., Herrmann, R.B., and Stauder, W., 1991, Seismotectonics of the Central United States, *in* Slemmons, D.B., Engdahl, E.R., Zoback, M.D., and Blackwell, D.D., eds., Neotectonics of North America: Boulder, Colo., Geological Society of America, p. 245–260.

Nuttli, O.W., Stauder, W., and Kisslinger, C., 1969, Travel time tables for earthquakes in the Central United States: Earthquake Notes, v. 40, no. 4, p. 19–28.

Shumway, R.H., 1988, Applied Statistical Time Series Analysis: Englewood Cliffs, N.J., Prentice-Hall, 379 p.

Taylor, K.B., and Wuenscher, M.E., 1990, Special investigations of seismic activity: The Ripley, Tenn. earthquake of 29 Aug. 1990 and the New Hamburg, Missouri earthquake of 26 Sept. 1990, *in* Central Mississippi Valley Earthquake Bulletin: Quarterly Bulletin 66, Third Quarter 1990, Saint Louis University.

Yang, Y.T., Chiu, J.M., Chen, K.C., Liaw, Z.S., Chiu, S.C., and Johnston, A.C., in press, Single-event, first motion, focal mechanism studies in the central NMSZ using PANDA data: Bulletin of the Seismological Society of America, v. 85.

Zhao, L.-S., and Helmberger, D.V., 1994, Source estimation from broadband regional seismograms: Bulletin of the Seismological Society of America, v. 84, no. 1, p. 91–104.

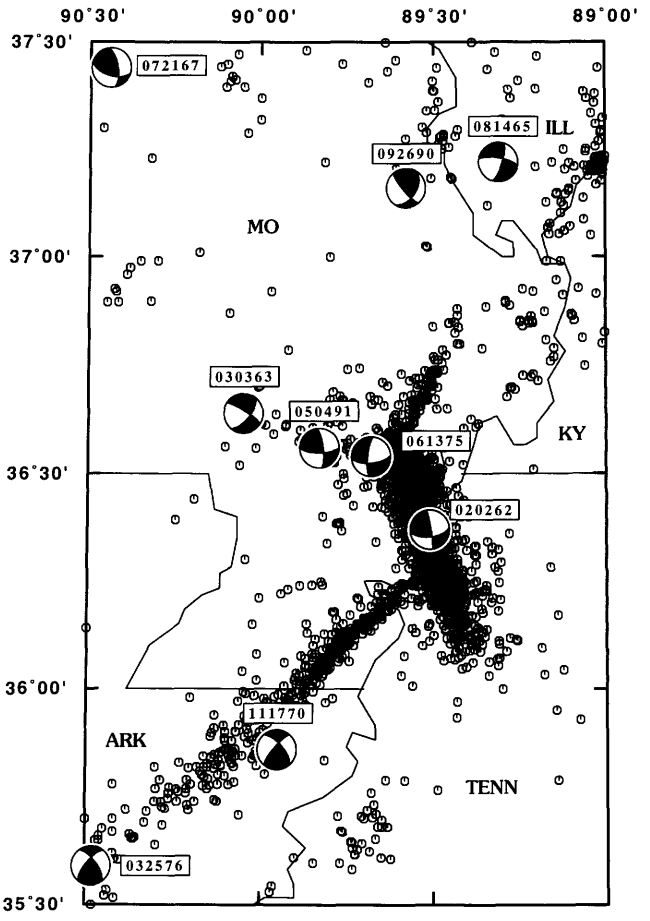

Figure 8. Surface-wave focal mechanisms from this study and Herrmann (1979b, in press) in the New Madrid region superimposed on regional-seismic-network epicenters. Dates of occurrence are shown with focal-mechanism plots (i.e., 050491 indicates May 4, 1991).

Zoback, M.D., and Zoback, M.L., 1991, Tectonics stress field of North America and relative plate motions, *in* Slemmons, D.B., Engdahl, E.R., Zoback, M.D., and Blackwell, D.D., eds., Neotectonics of North America: Boulder, Colo., Geological Society of America, p. 339–366.

Zoback, M.L., 1992, Stress field constraints on intraplate seismicity in eastern North America: Journal of Geophysical Research, v. 97, no. B8, p. 11761–11782.

Published in the Central Region, Denver, Colorado
Manuscript approved for publication December 21, 1994
Edited by Richard W. Scott, Jr.
Graphics prepared by Carol Quesenberry
Photocomposition by Patricia L. Wilber

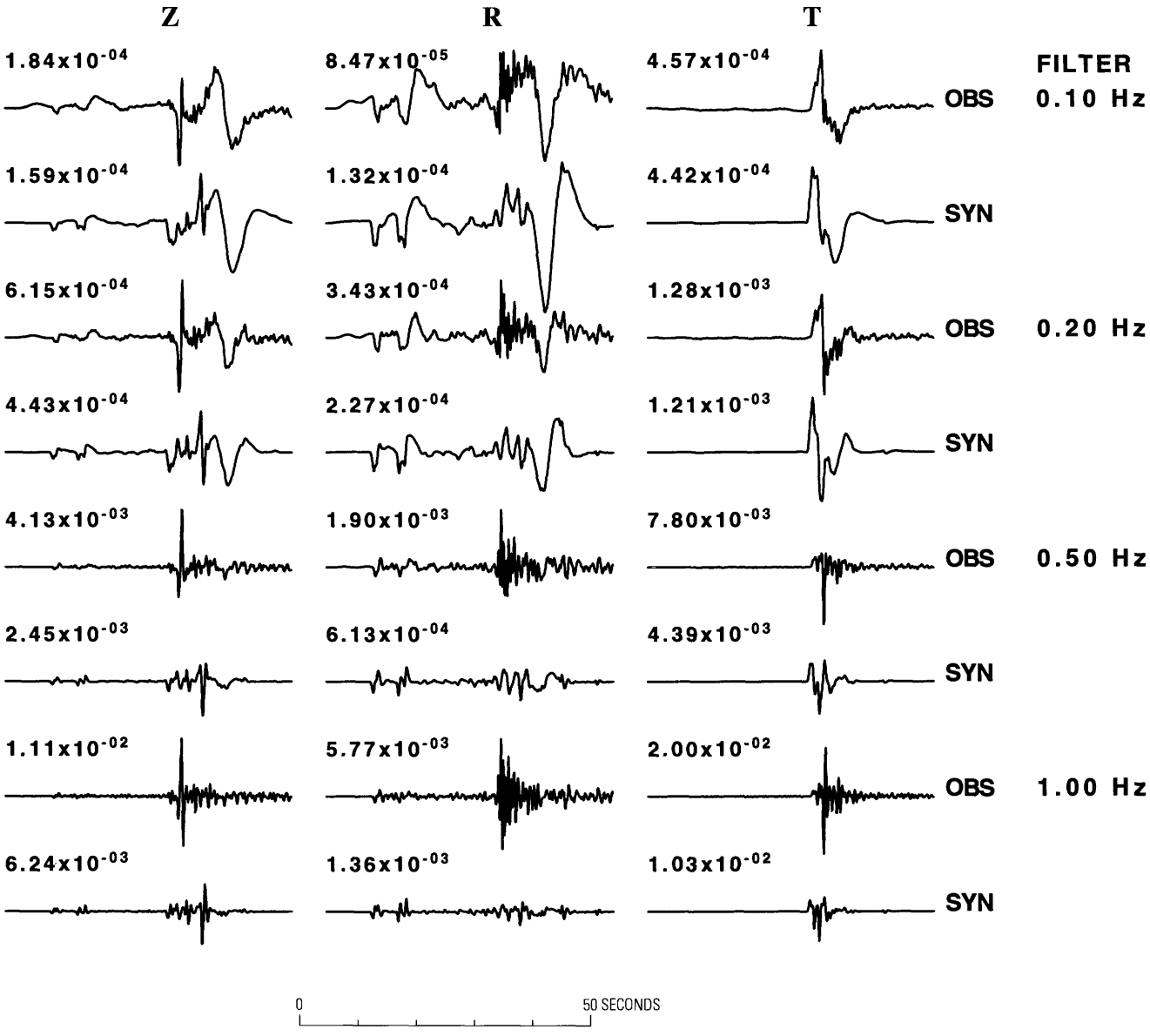

Figure 9. Comparison of filtered observed (OBS) and CUS model synthetic (SYN) three component ground-velocity time histories for the September 26, 1990, earthquake. The broadband velocity time histories, in units of cm/s, are low-pass-filtered at 0.10, 0.20, 0.50 and 1.00 Hz with a second-order Butterworth filter. For each component and each filter frequency, the same plotting scale is used to emphasize differences in peak values. All traces start 20 s after the origin time and consist of 50-s segments. Positive Z, R, and T component values represent motion up, away from the source, and in a direction clockwise around the source.

APPENDIX

GRID SEARCH

For focal-mechanism determination, a grid search is used with goodness-of-fit criteria designed to quantify a good visual fit between observed and modeled time histories. Let the N-sample synthetic and observed three-component time histories for the Z, R, and T components be s_Z, s_R, s_T and o_Z, o_R, o_T, respectively, where the synthetic time histories are generated for a unit seismic moment and a given combination of strike, dip, and rake angles and source depth. Because the waveforms may not agree in time due to either the Earth model used for synthetics or seismograph timing, the first step is to determine the time shift required to align the prominent features of the two time series.

Construct theoretical and observed vectors of time histories by concatenating the respective components:

$$\boldsymbol{s} = (s_Z, s_R, s_T) \tag{1}$$

and

$$\boldsymbol{o} = (o_Z, o_R, o_T) \tag{2}$$

Note that these are equivalently 3N-dimensional vectors. A cross correlation of the two time series is used to define the required time shift. Next, the synthetic time series are shifted, and the shifted time series for each component defined by $\hat{s}_Z$, $\hat{s}_R$, and $\hat{s}_T$. The goodness of fit of each individual component is given by the vector dot product of the unit vectors:

$$r_c = \hat{s}_c \cdot o_c / (|\hat{s}_c||o_c|) \tag{3}$$

for

$$c=Z, R, T$$

Following Zhao and Helmberger (1994), individual seismic-moment estimates are made for each component by using the relation

$$M_0{}^c = Max(|o_c|) / Max(|\hat{s}_c|) \tag{4}$$

Thus, for each choice of source depth and focal-mechanism parameters, six numbers are generated, $M_0{}^c$ and r_c, for $c=Z$, R, and T. To quantify the visual goodness-of-fit criteria, we require that the individual r_c be as close to 1 as possible and that the individual seismic-moment estimates be equal. Mathematically, this can be expressed by defining the three-component vectors $\mathbf{r}=(r_Z, r_R, r_T)$, $\mathbf{M}=(M_0{}^Z, M_0{}^R, M_0{}^T)$, and $\mathbf{1}=(1, 1, 1)$, and the numbers

$$r_g = \mathbf{M} \cdot \mathbf{1} / (|\mathbf{1}||\mathbf{M}|) \tag{5}$$

and

$$r_b = \mathbf{r} \cdot \mathbf{1} / (\mathbf{1} \cdot \mathbf{1}) \tag{6}$$

r_g measures the similarity of moment estimates, and r_b measures the closeness of individual elements of $\mathbf{r}$ to unity.

The best fit is that which maximizes the product $RB=r_b r_g$. The seismic-moment estimate is the weighted average

$$M_0 = \mathbf{r} \cdot \mathbf{M} / (\mathbf{r} \cdot \mathbf{1}) \tag{7}$$

There are several advantages to the techniques proposed. First, even though the example considers a fit to a three-component time history, the mathematical steps will work for a single-trace comparison or for many traces from many stations. In this latter case, individual r_c and $M_0{}^c$ values are determined for each station, but the $\mathbf{r}$, $\mathbf{M}$, and $\mathbf{1}$ vectors would have a dimension greater than 3. The formulation for the goodness-of-fit parameter and the weighted seismic-moment estimate would remain the same. The second point is that the formalism permits the application of a time-dependent weighting function to each observed-synthetic trace pair for the purpose of enhancing low-amplitude, but significant, arrivals, such as P and sP relative to S and the surface wave. The only negative about this procedure is that it is very computationally intensive compared to the simple comparison of first-motion and amplitude-ratio data that Langston (1994) used as an initial inversion.

Figure 10 shows an example of graphical output of the program that implements the goodness-of-fit estimation. The top row shows the concatenated Z, R, and T theoretical traces for the source parameters and seismic moment of 1.0×10^{20} dyne-cm. The result is a time series 150 s long. The second row gives the corresponding observed time series. The vertical tick marks indicate the termination points of individual components. The bottom row shows the cross-correlation function, which indicates a 2.3-s time shift between the top two traces. The traces are not exactly identical in shape because the autocorrelation function is not perfectly symmetric about its maximum. The third row superimposes these traces after shifting the observed trace by –2.3 s. Above each component are the individual component goodness-of-fit values and seismic moment estimates, e.g., r_Z=0.906 and $M_0{}^Z=1.943\times10^{22}$, respectively, for the Z component. The overall goodness-of-fit is RB=0.871, and the mean moment estimate is $M_0=2.01\times10^{22}$ dyne-cm.

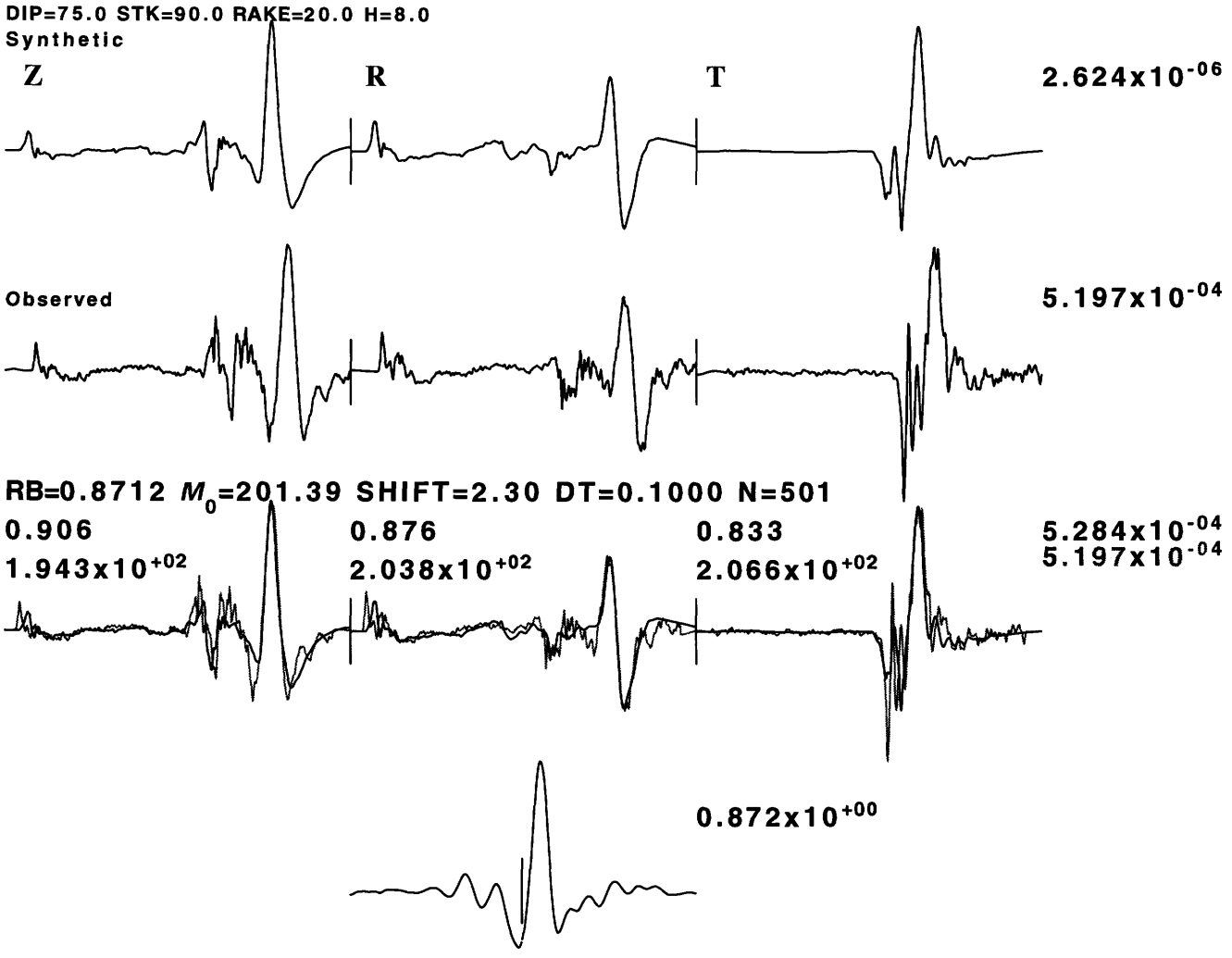

Figure 10. Graphic example of mathematical operations used in the determination of goodness-of-fit in the grid search technique. The first and second rows show the concatenated Z, R, and T time histories of the synthetic and observed 15-100 WWSSN seismograms for the May 5, 1991, earthquake recorded at CCM. The synthetics were generated using the CUS model (table 2), a dip of 75°, a strike of 90°, a rake of 20°, a depth of 8 km, and a seismic moment of 1.0×10^{20} dyne-cm. The bottom row shows the cross-correlation function. The third row shows the superposition of the observed (gray) and synthetic (solid) traces after time shifting and peak-amplitude normalization. Annotations on the third row indicate: the individual component correlation coefficient and moment estimate (e.g., 0.906 and 194.3 for the Z component); the overall goodness-of-fit, RB; the moment estimate relative to that used to generate the synthetic, M_0; the required time shift; the data sampling interval; and the number of points sampled for each component. Vertical ticks are used to separate individual components. Positive Z, R, and T component values represent motion up, away from the source, and in a direction clockwise around the source.

SINGLE-STATION PHASE-VELOCITY ESTIMATE

Given a known seismic source defined in terms of its moment tensor and distribution of point forces, synthetic seismograms can easily be generated for plane-layered, isotropic media. If the observed signal and the synthetic consist of a well-defined fundamental-mode surface wave, then the difference in the complex phase of the signals can be used to define the phase velocity of the observed surface wave, which in turn can be inverted for an improved velocity model. This section describes a cross-correlation technique to estimate the phase velocity and, more importantly, to provide a qualitative estimate of the confidence in the dispersion.

For simplicity, let the synthetic fundamental-mode signal have a Fourier transform $X(f)$ expressed as

$$X(f) = A(f)\, e^{i\phi(f)}\, e^{-ik(f)r} \tag{8}$$

where

r is the source-receiver distance,

$A(f)$ and $\phi(f)$ includes the effect of source time function and surface-wave excitation, and

$k(f)$ is related to the phase velocity, $c(f)$, by $k(f)=2\pi f/c(f)$.

Let the observed signal be given by

$$Y(f) = A_o(f)\, e^{i\psi(f)} \tag{9}$$

If the observed signal only consists of the fundamental-mode surface wave, which is possible through appropriate time-domain windowing or phase-match filtering, then

$$Y(f) = A_o(f)\, e^{i\Phi(f)}\, e^{-iK(f)r} \tag{10}$$

If it is assumed that the source is known, e.g., $\Phi=\phi$, then the simple mathematical technique of cross-correlation can be used to define the difference in phase,

$$\frac{Y(f)\,X^*(f)}{X(f)\,X^*(f)} = \frac{A_o(f)}{A(f)} e^{-i[K(f)-k(f)]r} \tag{11}$$

where

the * symbol represents a complex conjugate.

The phase of the left-hand side can be interpreted in terms of the difference in wavenumber and, effectively, the phase velocity between the observed and synthetic traces.

If the assumptions of knowing the source phase and having only a single mode in the observed signal are not met, then the inferred phase-velocity correction cannot be accepted with confidence. This difficulty can be addressed by using smoothed spectra, and a statistical test (Jenkins and Watts, 1968; Shumway, 1988).

The time series $x(t)$ and $y(t)$ are windowed between a t_{min} and t_{max} to isolate the surface-wave mode and then Fourier-transformed to provide windowed complex Fourier spectra, $X(f)$ and $Y(f)$. From these two spectra, the autocorrelation and cross-correlation spectra are defined from the relations

$$XY(f) = Y(f)\,X^*(f) \tag{12}$$

$$XX(f) = X(f)\,X^*(f) \tag{13}$$

$$YY(f) = Y(f)\,Y^*(f) \tag{14}$$

The smoothed spectra $\overline{XY}$, $\overline{XX}$, and $\overline{YY}$, at a frequency $f=k\Delta f$ are defined by

$$\overline{XY}(k) = \frac{1}{L} \sum_{n=-(L-1)/2}^{(L-1)/2} XY(k+n) \tag{15}$$

the coherency squared, κ_{12}^2,

$$\kappa_{12}^2 = \left|\overline{XY}\right|^2 / \left(\overline{XX}\,\overline{YY}\right) \tag{16}$$

and the estimated cross spectra

$$\overline{H}(f) = \bar{A}(f)\, e^{i\bar{\Phi}(f)} = \overline{XY}(f) / \overline{XX}(f) \tag{17}$$

Because of the smoothing, there is redundant information that can be used to estimate the confidence on the cross spectra. The statistical test is whether the two spectra are significantly different. Defining a factor

$$\Phi = \left(\frac{2}{2(L-1)} f_{2,2(L-1)}\,(1-\alpha)\,(1-\kappa_{12}^2)/\kappa_{12}^2 \right)^{1/2} \tag{18}$$

then the $100(1-\alpha)$ percent confidence bands on the amplitude and phase spectrum of the cross spectrum are

$$\bar{A}(f)\,(1 \pm \Phi) \tag{19}$$

$$\bar{\phi}(f) \pm \sin^{-1}(\Phi) \tag{20}$$

To estimate the phase velocity and error, let r be the distance between the two surface-wave observations, and let the theoretical phase velocity used to generate the synthetic be c_m. The difference in the phase will be explained by a difference in phase velocities. The corrected phase-velocity estimate is obtained from

$$\frac{1}{c} = \frac{1}{c_m} - \frac{\bar{\phi}(f)}{\omega r} \tag{21}$$

and the error in the phase velocity is estimated to be

$$\Delta c = c^2 \sin^{-1}(\Phi) / \omega r \tag{22}$$

Experimentation shows that increasing the smoothing window will reduce the coherency, and, hence, increase the 95-percent confidence limits on the phase velocity. A value of $L=3$ is adequate. In addition, a larger L will lead to rippling in the phase velocity at high frequencies, which may be due to the use of an essentially rectangular smoothing function.

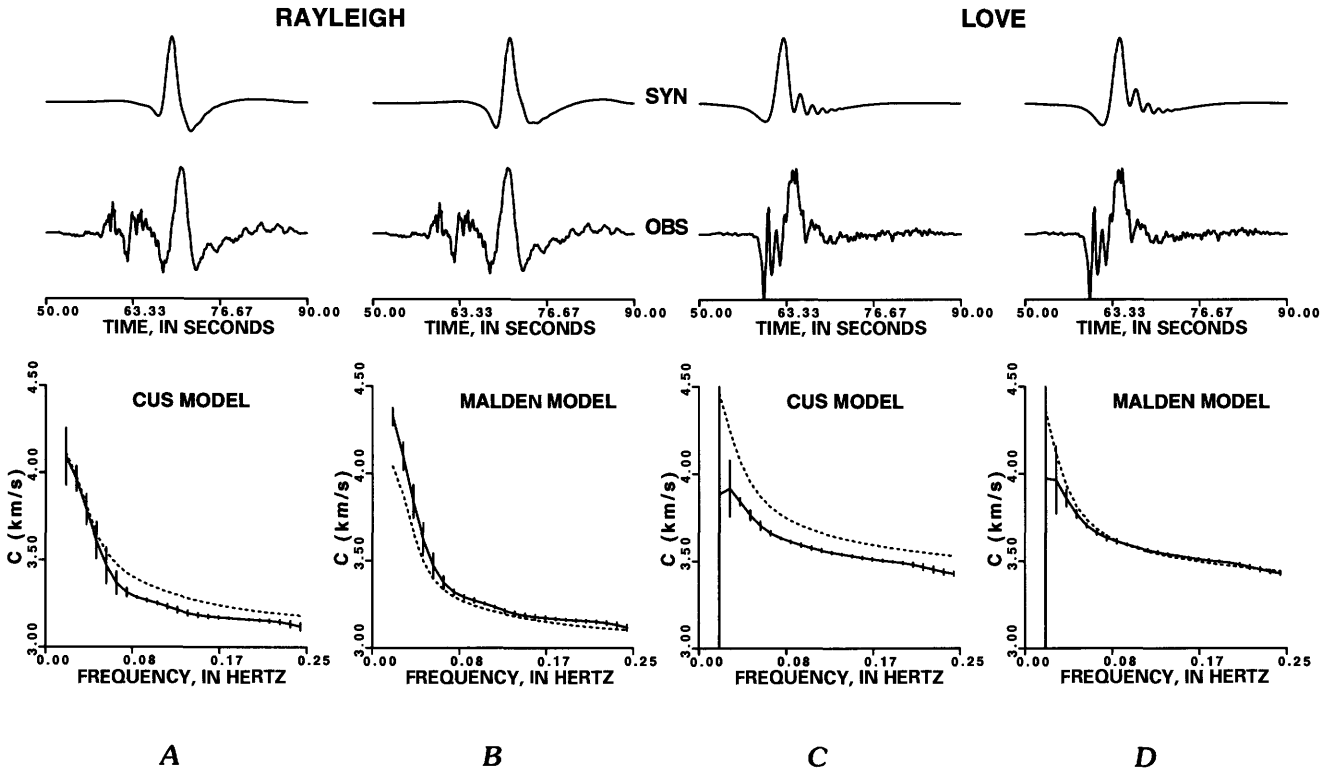

Figure 11. Demonstration of the cross-correlation technique used to revise the initial Earth structure model between the May 4, 1991, earthquake and the CCM station. A and C illustrate the modification of the original dispersion computed using the CUS model for the Rayleigh and Love waves, respectively. The top traces are the synthetics predicted using the CUS model, and the second set of traces are the observed data. The dotted lines in the phase velocity versus frequency plots are the theoretical phase-velocity dispersions based on the CUS model, and the solid lines with error bars are the dispersions required to explain the signal differences in shape and arrival time. The new dispersion was inverted to yield the MALDEN model of table 2. B and D show the result of another iteration starting with the MALDEN model of table 2. The results indicate little need to change that portion of the model affecting dispersion between 0.05 and 0.25 Hz. All traces have been passed through a WWSSN 15-100 long-period instrument.

This technique was applied to the observed vertical (Z) and tangential (T) traces for the May 4, 1991, earthquake. Figure 11 shows the windowed WWSSN 15-100 long-period instrument time histories. No attempt was made to isolate the fundamental mode using phase-match filters.

Consider Figure 11*A*, which compares the theoretically predicted vertical-component Rayleigh-wave arrival for a depth of 8 km and the mechanism given in table 1 using the CUS model of table 2 to the observed signal at CCM. The model-predicted dispersion is given by the dotted curve, whereas the dispersion inferred using the cross-correlation analysis is given by the solid curve with error bars. As is obvious from the signals, the CUS model is too fast. In addition, the shape of the Rayleigh-wave pulse differs. Figure 11*C* is a similar display for the Love wave. The resulting dispersion curves were inverted by starting with the CUS model and keeping Poisson's ratio fixed. The Δc values are used as relative weights in the inversion. The new Earth model is given as the MALDEN model in table 2. Figures 11*B* and 11*D* show the result of further processing with this newer model for the Rayleigh and Love arrivals, respectively. First note that the arrival times of the positive peaks of the waveforms now agree and that little additional change in the dispersion is required in the 0.04- to 0.25-Hz band. Because the improved fit yielded better waveform shapes, no further iterations were performed.

☆ U.S. GOVERNMENT PRINTING OFFICE: 1995 - 673-046 / 20004 REGION NO. 8